Available online at www.sciencedirect.com
ScienceDirect
Geochimica et Cosmochimica Acta 70 (2006) 4513–4527
Geochimica
www.elsevier.com/locate/gca

Trace element partitioning between apatite and silicate melts

Stefan Prowatke [a,1], Stephan Klemme [b,c,*]

[a] Mineralogisches Institut, Universität Heidelberg, Im Neuenheimer Feld 236, 69120 Heidelberg, Germany
[b] Centre for Science at Extreme Conditions, University of Edinburgh, Erskine Williamson Building, Mayfield Road, Edinburgh EH9 3JZ, UK
[c] School of GeoSciences, University of Edinburgh, The Grant Institute, West Mains Rd., Edinburgh EH9 3JW, UK

Received 6 December 2005; accepted in revised form 14 June 2006

Abstract

We present new experimental apatite/melt trace element partition coefficients for a large number of trace elements (Cs, Rb, Ba, La, Ce, Pr, Sm, Gd, Lu, Y, Sr, Zr, Hf, Nb, Ta, U, Pb, and Th). The experiments were conducted at pressures of 1.0 GPa and temperatures of 1250 °C. The rare earth elements (La, Ce, Pr, Sm, Gd, and Lu), Y, and Sr are compatible in apatite, whereas the larger lithophile elements (Cs, Rb, and Ba) are strongly incompatible. Other trace elements such as U, Th, and Pb have partition coefficients close to unity. In all experiments we found $D_{Hf} > D_{Zr}$, $D_{Ta} \approx D_{Nb}$, and $D_{Ba} > D_{Rb} > D_{Cs}$. The experiments reveal a strong influence of melt composition on REE partition coefficients. With increasing polymerisation of the melt, apatite/melt partition coefficients for the rare earth elements increase for about an order of magnitude. We also present some results in fluorine-rich and water-rich systems, respectively, but no significant influence of either H_2O or F on the partitioning was found. Furthermore, we also present experimentally determined partition coefficients in close-to natural compositions which should be directly applicable to magmatic processes.

1. Introduction

Apatite is an ubiquitous accessory phase in many magmatic, metamorphic, and sedimentary rocks (Beswick and Carmichael, 1978; Raimbault et al., 1993; Sorensen and Grossman, 1993; Bea et al., 1994; Haggerty et al., 1994; Piccoli and Candela, 1994; Dawson et al., 1996; D'Orazio et al., 1998; Yaxley et al., 1998; Nag et al., 1999; Seifert et al., 2000; Amelin and Zaitsev, 2002; Dawson, 2002; O'Reilly and Griffin, 2002; Dawson and Hinton, 2003; Brigatti et al., 2004; Parat and Holtz, 2004; Nishizawa et al., 2004). As naturally occurring apatites contain large amounts of the rare earth elements and Sr, it has been well known that apatite controls a large portion of the budget of these trace elements. Recent studies also indicate that apatite may also contain significant amounts of U and Th (Dawson et al., 1996; O'Reilly and Griffin, 2002; Dawson and Hinton, 2003) and may, therefore, be a major host of these elements in the mantle or the crust. If apatite stays residual during mantle melting it may fractionate these element during partial melting. Moreover, apatite may control REE, U, and Th budgets of primitive basalts by contamination when these primitive melts interact with the crustal lithosphere during ascent from the source in the mantle to the surface (O'Reilly and Griffin, 2002).

Apatite saturation in magmatic systems has been studied extensively (Watson, 1979; Watson, 1980; Watson and Green, 1981; Harrison and Watson, 1984; Kogarko et al., 1988; Ryabchikov et al., 1991; Pichavant et al., 1992; Wolf and London, 1994), however, there is only very little experimental information as to how trace elements partition between silicate melts and apatite (Watson and Green, 1981). Watson and Green (1981) found in an experimental study that REE and Sr are strongly compatible in apatite. Since then, however, only one experimental study was conducted to investigate the partitioning of trace elements between apatite and carbonatite melt (Klemme and Dalpe, 2003). As the melt composition in Klemme and Dalpe's experiments is very different from silicate systems, the

* Corresponding author.
E-mail address: stephan.klemme@ed.ac.uk (S. Klemme).
[1] Present address: Swarovski, 6112 Wattens, Austria.

0016-7037/$ - see front matter © 2006 Elsevier Inc. All rights reserved.
doi:10.1016/j.gca.2006.06.162

applicability of these results to granitic or andesitic rocks needs to be tested.

There are also a number of so-called mineral/matrix partition coefficients in the literature which are calculated from naturally occurring mineral phenocrysts and a matrix which is often volcanic. We believe that mineral/matrix partition coefficients are much more difficult to interpret when compared to experimentally derived partition coefficients. This is caused by the fact that natural rock matrix compositions are often heterogenous and their bulk compositions are consequently only poorly constrained when compared to an experimental run product. Furthermore, the attainment of equilibrium between crystals and melts in natural phenocryst/matrix systems is only difficult to ascertain. Moreover, phenocryst/matrix partition coefficients are determined in natural compositions with often very low concentration of the trace element of interest, which means that analyses of phenocrysts are often very close to the analytical detection limit and consequently suffer from large analytical uncertainties. However, the interested reader is referred to some previous studies on apatite phenocryst/matrix partition coefficients, some of which are in good agreement with our experimental data and some are not (Nagasawa, 1970; Nagasawa and Schnetzler, 1971; Paster et al., 1974; Fujimaki, 1986; Mahood and Stimac, 1990; Bea et al., 1994; Chazot et al., 1996; D'Orazio et al., 1998).

2. Experimental and analytical techniques

2.1. Experimental rationale

We set out to investigate trace element partition coefficients between apatite and silicate melts, many of them hitherto unknown. We chose a number of different bulk compositions to approximate basaltic to andesitic bulk composition (see Section 2.2). As our experiments were performed with very different melt compositions, we also set out to investigate the influence of melt composition on partition coefficients (Prowatke and Klemme, 2005, 2006). Most experiments were performed in water-bearing composition with hydroxylapatites. However, to investigate a possible effect of fluorine on partition coefficients, some experiments were run in F-rich bulk compositions with F-apatites.

2.2. Starting materials

The starting materials consisted of mechanical mixes of synthetic oxides (MgO, Fe_2O_3, $CaCO_3$, Na_2CO_3, K_2CO_3, Al_2O_3, and SiO_2). Several bulk compositions were prepared (Table 1). MgO and Al_2O_3 were initially fired at 1050 °C to drive off any residual moisture. All starting materials were stored at 110 °C. Subsequently, a trace element cocktail, consisting of pure oxides and carbonates of 18 trace elements (Rb, Sr, Y, Zr, Nb, Cs, Ba, La, Ce, Pr, Sm, Gd, Lu, Hf, Ta, Pb, Th, and U) was then added. The starting material mixtures were then ground under acetone in an

Table 1
Major element (wt%, nominal) composition of starting materials

	ASI200	ASI220	ASI240	SH4 basalt	SH3 basaltic andesite	SH3Fe basaltic andesite	SH3M basaltic andesite	SH2 andesite	Liquid–liquid
SiO_2	67.81	66.36	64.96	46.00	53.50	53.50	53.50	65.30	76.90
Al_2O_3	6.58	11.90	17.01	20.00	17.70	17.70	17.70	18.20	15.00
Na_2O	20.99	17.21	13.59	1.50	2.80	2.80	2.80	4.80	3.40
K_2O	1.52	1.49	1.45	0.50	1.80	1.80	1.80	3.90	4.70
CaO	1.81	1.77	1.73	15.00	12.40	12.40	12.40	7.80	—
MgO	1.30	1.27	1.25	17.00	11.80	4.30	6.50	—	—
FeO	—	—	—	—	—	7.50	5.30	—	—
Total	100.0	100.0	100.0	100.0	100.0	100.0	100.0	100.0	100.00
Addition of phosphate component									
Exp.	#43 31% FAp	#5426% FAp		#48A35% FAp					
Exp.	#7235 % OHAp5%	#7830 %OHAp5% H_2O	#7725% OHAp5%H_2O		#59A25% OHAp5% H_2O	#61A25% OHAp5% H_2O	#71A25% OHAp5% H_2O	#61B18% OHAp5% H_2O	(L–L20%$Ca_2P_2O_7$)

FAp = $Ca_{5.5}(PO_4)_3F_2$: consists of a mixture between 1.5 mol $Ca_3(PO_4)_2$ and 1 mol CaF_2; OHAp = $Ca_5(PO_4)_3OH$ (Merck, GmbH).

agate mortar to produce homogeneous mixtures. These mixtures were decarbonated at 1000 °C for 4 h, melted in air at 1400 °C and subsequently at 1600 °C, and then quenched to a glass. This procedure was repeated several times, with fine grinding in between. Various amounts of synthetic $Ca_3(PO_4)_2$, CaF_2, or $Ca_5(PO_4)_3OH$ were then added to these compositions. The resulting mixtures were mixed again and stored at 110 °C, without melting again. The major element compositions of the starting materials and the added amounts of phosphate are given in Table 1.

2.3. Experimental procedures

The experiments were carried out at 1.0 GPa in a conventional end loaded 1.27 cm piston-cylinder apparatus at Heidelberg University. The pressure assembly consists of two inner parts of crushable alumina surrounded by concentric shells of a graphite heater, a soft glass tube of Duran© (Schott AG, Germany) and an outermost sleeve of natural talc. This assembly requires a friction correction of −11%, calibrated on the fayalite–quartz–ferrosilite and the $MgCr_2O_4 + SiO_2 = Cr_2O_3 + Mg_2SiO_4$ equilibria (Bohlen et al., 1980; Klemme and O'Neill, 1997; Klemme et al., 2002). The runs were performed using the hot "piston-in" routine. First,a pressure of about 0.25 GPa was applied. Then the sample was heated up to about 550 °C to soften the glass. During the final compression, pressure and temperature were raised simultaneously. Pressure was kept constant automatically during runs to within ±0.05 GPa. Starting materials were sealed into graphite-lined platinum capsules, which were placed in holes in the lower alumina inner part and separated from the thermocouple by a thin Al_2O_3 disc. The use of graphite inner capsules should minimize the loss of Fe to the noble metal capsule and ensure reducing conditions close to the C–CO oxygen buffer. Temperatures were measured with calibrated $W_{95}Re_5$–$W_{75}Re_{25}$ thermocouples inserted axially into the assembly using four-bore high-purity Al_2O_3 tubing. No correction was made for the dependence of thermocouple emf on pressure. The sample was placed in the hotspot of the assembly, and temperature uncertainties were calibrated to be less than 15 °C. All experiments were initially heated above their liquidus and subsequently cooled at different rates (50–100°/h) to 1250 °C (see Table 2). These particular temperatures were chosen because no other phases were found to exist next to apatite and the melt fraction in the experimental run products is usually much greater than 50%. Samples were held at the final run temperature for a duration of up to 20 h to allow equilibration of crystalline phases and coexisting melts (see Table 2 for details). Moreover, one additional silicate liquid–phosphate liquid experiment in the system SiO_2–Al_2O_3–Na_2O–K_2O–CaO–P_2O_5 (Krigman and Krot, 1992) was carried out to further constrain melt compositional effects on trace element partitioning (Table 1). The trace element cocktail was indentical to that used for the high pressure experiments. The liquid–liquid partitioning experiment was run at atmospheric pressure in a large Pt crucible at 1510 °C for 45 min.

2.4. Analytical techniques

Experimental run products were sectioned longitudinally with a miniature diamond saw, and one half mounted in epoxy and carefully polished with a series of water-based diamond pastes. Polished sections were carbon coated for electron microprobe analysis. Glasses were analysed for major elements with a Cameca electron microprobe (SX51) at Heidelberg University operated using an accelerating voltage of 15 kV and a beam current of 6 nA. To minimize alkali volatility and a "damage" to glasses under the electron beam an area of 10 × 12 μm was scanned with a 1 μm beam. Counting times were 10 s on peak and 5 s on background for all elements. Major element concentrations of apatites were also determined with the electron microprobe. For mineral analyses an accelerating voltage of 15 kV, a beam current of 20 nA, and a beam with 1 μm in diameter were used. The counting times were identical, except for the minor elements Si, Na, Fe, Mg, F, and Al with 40 s on peak and 20 s on background. The standards used were albite (Na), K-feldspar (K), corundum (Al), periclase (Mg), wollastonite (Ca, Si), fluorite (F), and synthetic apatite (P). The raw data were corrected with the 'PAP' software (Pouchou and Pichoir, 1985).

Trace element concentrations were determined by secondary ion mass spectrometry (SIMS) on a Cameca ims

Table 2
Experimental run conditions

Experiment	Starting temperature	Run temperature	Ramp (°C/h)	Run duration at final T (h)	Start material	Crystal shape	Size (μm)
72	1450	1250	50	4	ASI200	Euhedral	100 × 100
78	1400	1250	50	17	ASI220	Euhedral	80 × 50
77	1400	1250	50	18	ASI240	Euhedral	50 × 50
61B	1500	1250	100	15	SH2	Euhedral	20 × 20
71A	1350	1250	50	6	SH3M	Euhedral	50 × 40
61A	1500	1250	100	15	SH3Fe	Euhedral	60 × 50
48B	1450	1250	50	16.5	SH4F	Euhedral	80 × 60
43	1450	1250	50	17	ASI200F	Euhedral	50 × 50
54	1450	1250	50	19.5	ASI220F	Euhedral	60 × 70
59	1400	1250	50	5	SH3	Euhedral	80 × 80
60B	1450	1250	50	16	SH4	Euhedral	15 × 15

3f ion microprobe at Heidelberg University, using a nominal 10 kV primary beam of $^{16}O^-$ ions. Positive secondary ions were accelerated to 4.5 keV. The energy window was set at 40 eV. We employed the energy filtering technique with an offset of 90 eV at a mass resolution M/ΔM (10%) of ≈400 to suppress interfering molecules and to minimise matrix effects. The primary current was 20 nA, resulting in a spatial resolution of ca. 20–25 μm diameter at the sample surface. The following masses were counted: ^{44}Ca, ^{85}Rb, ^{88}Sr, ^{89}Y, ^{90}Zr, ^{93}Nb, ^{133}Cs, ^{138}Ba, ^{139}La, ^{140}Ce, ^{141}Pr, ^{149}Sm, ^{160}Gd, ^{175}Lu, ^{178}Hf, ^{181}Ta, ^{208}Pb, ^{232}Th, ^{238}U, and ratioed to ^{44}Ca, as determined by EMPA. Ion yields were calibrated on synthetic Ca–P glass. The trace element concentrations of this synthetic glass were independently determined with LA-ICPMS techniques at the University of Frankfurt and used to determine elemental ion yields needed for standardisation during SIMS analyses. These ion yields were compared to the ion yields that were determined using the reference material NIST SRM 610 (Pearce et al., 1997). The differences between these ion yields usually are much less than 10–15% relative for most elements, with one notable exception for Pb on the synthetic Ca–P glass. Partition coefficients determined with LA-ICPMS agree well with results from SIMS measurements (Fig. 1).

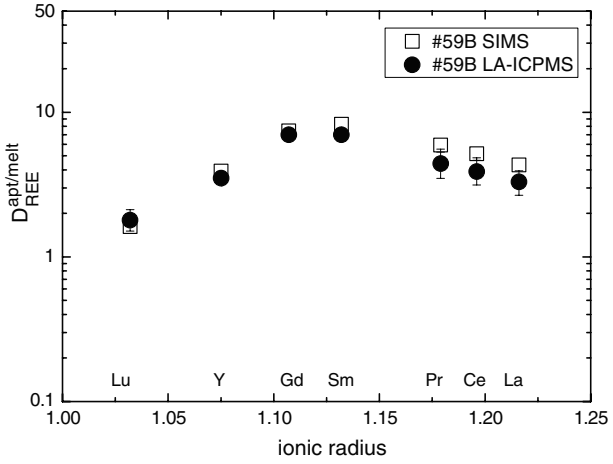

Fig. 1. Comparison of D_{REE} values calculated from SIMS analyses (open squares) and LA-ICPMS analyses.

3. Results and discussion

3.1. Experimental results

Experimental run products of all experiments consisted exclusively of euhedral apatites and quenched melts, with exception of experiment #72 where an additional large nearly anhedral whitlockite crystal was found to coexist with apatite and melt. In all experiments, modal proportions of crystals are less than 30%. The largest apatites were 100 × 100 μm across, and were found in the experiments with the lowest degree of polymerisation of melts (Fig. 2 (A) run #43, (B) run #72). No inclusions of other phosphate phases were found in apatite, but small rounded inclusions of quenched melt are occasionally observed. We found no connection between the degree of polymerisation of the melt and the number of melt inclusions and the shape of the crystals. All experiments were free of vesicles and quench crystals.

Major and trace element composition of the apatites from all experiments are listed in Table 3. Although the experiments are unreversed (as in most other trace element partitioning studies and melting equilibria studies), there is evidence that equilibrium was attained in our experiments as mineral and glass analyses have low standard deviations indicating homogenous, unzoned phases (Table 3).

The Si content in apatite is low and varies between 0.01 and 0.07 cations per formula unit (cpfu). The exception was experiment 60B, where a Si content of 0.15 cpfu in apatite was observed. The Na content in apatite is also low and ranges between <0.01 and 0.10 cpfu. The Mg and Fe a content seems to depend on the Mg and Fe content of the melt, and varies between <0.01 and 0.10 and ~0.015 cpfu, respectively. The Ca and P content of the apatites show no systematic variation with changing bulk composition. We conclude that the major element compositions of our apatites are constant (within the uncertainties). Glasses are homogeneous as indicated by the very low standard

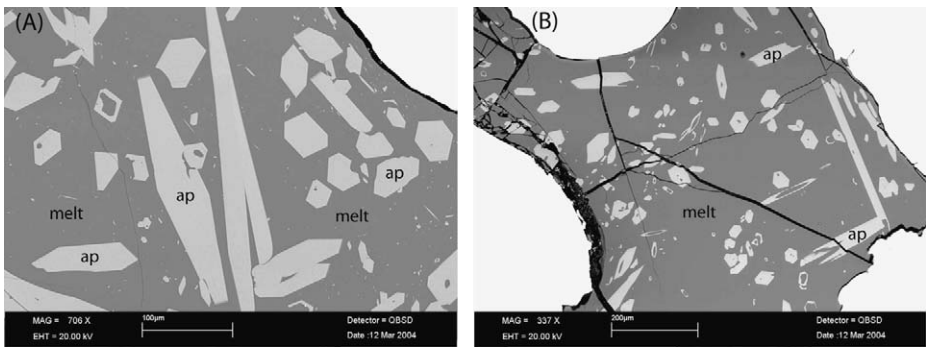

Fig. 2. Backscattered electron images of the experimental run products. (A) run products of experiment #43 (ASI200OH). The apatite crystals are euhedral and mostly are larger than 50 μm across. Only very few melt inclusions were found in these apatite crystals. (B) run products of experiment #54A (ASI220F). The apatites are euhedral but slightly smaller. Note that the cracks in all experimental run products are caused by quenching.

Table 3
Major element composition (wt%), unit formula (cpfu) and trace element content (ppm) of apatites

Sample n.o.a.	72 (6)	78 (6)	77 (6)	61B (9)	71A (9)	61A (7)	48B (9)	59B (5)	43 (5)	54A (3)	60B (A)
SiO_2	0.31(2)	0.33(2)	0.26(3)	0.55(4)	0.88(3)	0.45(4)	0.63(10)	0.59(5)	0.15(3)	0.25(7)	1.81(14)
Al_2O_3	0.00(−)	0.01(−)	0.02(−)	0.04(−)	0.04(−)	0.01(−)	0.01(−)	0.00(−)	0.01(−)	0.01(−)	0.09(1)
FeO	0.00(−)	0.02(−)	0.03(−)	0.02(−)	0.19(5)	0.29(6)	0.02(−)	0.01(−)	0.00(−)	0.00(−)	0.01(−)
MgO	0.01(1)	0.05(1)	0.13(3)	0.00(−)	0.49(1)	0.37(2)	0.94(2)	0.66(1)	0.01(−)	0.05(1)	1.09(4)
CaO	53.66(26)	53.74(19)	53.86(26)	54.59(30)	53.75(17)	54.15(21)	54.27(16)	54.06(19)	54.91(21)	54.94(21)	53.14(32)
SrO	0.02(−)	0.02(−)	0.03(−)	0.03(−)	0.01(−)	0.01(−)	0.02(−)	0.01(−)	0.03(−)	0.03(−)	0.00(−)
Na_2O	0.62(8)	0.60(3)	0.36(4)	0.11(2)	0.12(2)	0.05(−)	0.02(−)	0.05(−)	0.19(2)	0.14(3)	0.10(2)
P_2O_5	41.60(45)	41.22(40)	41.40(47)	41.04(25)	40.84(33)	41.38(44)	41.83(44)	41.06(27)	42.01(40)	42.12(31)	39.92(36)
F	0.00(−)	0.00(−)	0.00(−)	0.00(−)	0.00(−)	0.00(−)	4.13(17)	0.00(−)	4.29(34)	4.47(29)	0.00(−)
Cl	0.31(4)	0.54(1)	0.47(4)	0.06(2)	0.10(4)	0.07(1)	0.02(−)	0.02(−)	0.07(2)	0.05(2)	0.07(2)
F·Cl═O	0.07	0.12	0.11	0.01	0.02	0.02	1.74	0.01	1.82	1.89	0.02
Total	96.64	96.61	96.74	96.87	96.50	96.90	100.24	96.75	100.08	100.46	96.21
cpfu											
Na	0.1022	0.1001	0.0595	0.0184	0.0192	0.0086	0.0032	0.0082	0.0317	0.0223	0.0170
Ca	4.8923	4.9195	4.9197	4.9772	4.9001	4.9185	4.8638	4.9188	4.9551	4.9413	4.8440
Fe^{2+}	0.0002	0.0013	0.0022	0.0013	0.0134	0.0203	0.0012	0.0006	0.0003	0.0000	0.0009
Mg	0.0014	0.0058	0.0162	0.0000	0.0626	0.0466	0.1176	0.0830	0.0012	0.0057	0.1377
Sr	0.0009	0.0011	0.0015	0.0015	0.0006	0.0006	0.0011	0.0005	0.0016	0.0017	0.0000
REE	0.0052	0.0061	0.0091	0.0098	0.0027	0.0043	0.0016	0.0067	0.0069	0.0095	—
Th + U	0.0003	0.0002	0.0002	0.0024	0.0002	0.0001	0.0009	0.0017	0.0002	0.0002	—
Total	5.0025	5.0341	5.0085	5.0106	4.9989	4.9991	4.9894	5.0196	4.9970	4.9807	4.9996
Si	0.0264	0.0280	0.0219	0.0469	0.0751	0.0383	0.0529	0.0498	0.0130	0.0206	0.1536
Al	0.0002	0.0014	0.0017	0.0043	0.0037	0.0012	0.0006	0.0002	0.0008	0.0011	0.0092
P	2.9971	2.9818	2.9880	2.9565	2.9414	2.9698	2.9616	2.9518	2.9953	2.9931	2.8752
Total	3.0237	3.0112	3.0116	3.0076	3.0202	3.0093	3.0150	3.0018	3.0090	3.0148	3.0379
F	—	—	—	—	—	—	1.0700	—	1.1175	1.1611	—
Cl	0.0430	0.0750	0.0652	0.0082	0.0154	0.0091	—	—	0.0089	0.0073	0.0010
n.o.a	(3)	(3)	(3)	(1)	(3)	(2)	(3)	(4)	(3)	(4)	(−)
Rb	0.43(7)	0.59(3)	0.33(10)	0.37(−)	0.75(6)	0.27(3)	0.41(2)	0.30(12)	0.14(6)	0.25(2)	—
Sr	157(8)	196(12)	263(18)	254(−)	106(1)	101(1)	217(2)	93(1)	277(6)	295(15)	—
Y	141(1)	165(7)	269(9)	252(−)	92(4)	154(2)	184(3)	245(3)	201(1)	287(9)	—
Zr	2.78(8)	8.16(3)	8.92(15)	6.48(−)	7.60(12)	8.17(27)	6.29(18)	7.45(20)	2.06(1)	3.14(70)	—
Nb	0.38(3)	0.69(5)	0.94(9)	0.47(−)	1.39(10)	0.70(3)	0.26(4)	0.78(4)	0.14(6)	0.34(19)	—
Cs	0.05(1)	0.07(2)	0.03(1)	0.03(−)	0.04(2)	0.07(2)	0.04(1)	0.06(2)	0.05(2)	0.09(1)	—
Ba	34.0(8)	55.4(36)	53.7(56)	52.3(−)	22.1(13)	17.0(7)	28.4(18)	17.2(8)	60.9(19)	67.8(3)	—
La	246(1)	282(7)	391(6)	458(−)	101(5)	154(3)	152(2)	236(5)	327(5)	445(25)	—
Ce	209(1)	246(3)	358(9)	387(−)	114(4)	174(2)	255(4)	244(2)	311(12)	388(27)	—
Pr	227(1)	273(7)	393(6)	494(−)	116(4)	174(4)	216(1)	224(3)	290(9)	418(26)	—
Sm	269(1)	321(3)	479(7)	526(−)	155(3)	248(2)	251(3)	367(6)	339(15)	474(49)	—
Gd	241(7)	280(1)	424(7)	349(−)	106(4)	170(2)	246(7)	365(3)	310(11)	439(44)	—
Lu	61.6(3)	78.0(4)	138(12)	195(−)	48.2(25)	80.3(50)	78.2(22)	96.4(3)	95.0(31)	140(4)	—
Hf	0.48(9)	1.06(15)	1.07(13)	1.24(−)	1.72(14)	1.17(23)	1.33(12)	1.60(24)	0.60(1)	0.70(18)	—
Ta	0.30(1)	0.38(14)	0.67(10)	0.87(−)	0.83(40)	0.40(5)	0.32(4)	0.38(6)	0.70(30)	0.41(2)	—
Pb	5.7(3)	36.1(4)	61.4(12)	60.8(−)	33.5(89)	16.6(6)	8.3(4)	16.1(3)	4.92(8)	14.7(28)	—
Th	43.2(15)	54.6(2)	80.4(5)	124.7(−)	64.4(6)	53.2(2)	58.4(7)	98.6(4)	34.2(5)	40.6(7)	—
U	73.0(13)	39.7(3)	14.0(14)	987(−)	31.0(32)	13.2(1)	111(3)	690(41)	50.7(18)	51.5(16)	—

n.o.a, number of analyses (x); cpfu, cations per formula unit. All errors are 1σ, given as last significant digits in brackets. Major elements were analysed with the electron microprobe, whereas trace elements were analysed using SIMS techniques (see text for analytical details). Note that traces of chlorine are also present due to contamination of the starting materials.

deviations of major element analyses (Table 4). Trace element analyses of apatites vary much less than 10%, no zoning of trace elements was observed. Glasses are also homogeneous in terms of trace elements as low standard deviations of trace element analyses from different part of the coexisting glasses indicate (Table 4). Trace element variation of the glass analyses are <5%, except for Pb with ~10%.

3.2. Partition coefficients between apatite and melts

All our experimental partition coefficients are listed in Table 5 and shown in Fig. 3. We find all rare earth elements (REE) to be compatible in apatite ($D > 1$), with the middle REE more strongly partitioning into apatite compared to the light REE or the heavy REE. This overall pattern is in excellent agreement with previous results by Watson and

Table 4
Major element composition (wt%) and trace element content (ppm) of quenched melts

Sample	72	78	77	61B	71A	61A	48B	59B	43	54A	60B
n.o.a.	(30)	(30)	(30)	(30)	(30)	(30)	(30)	(30)	(30)	(30)	(30)
SiO_2	52.89(43)	56.80(19)	56.16(28)	61.51(76)	50.15(23)	47.25(17)	40.70(22)	44.67(62)	57.15(27)	59.00(29)	35.87(23)
Al_2O_3	5.14(11)	9.93(8)	14.25(40)	15.90(19)	16.27(20)	15.14(15)	16.03(16)	13.95(25)	5.78(8)	10.86(11)	15.02(19)
FeO	b.d.	b.d.	b.d.	b.d.	2.18(21)	5.00(10)	b.d.	b.d.	b.d.	b.d.	b.d.
MgO	0.99(7)	1.12(5)	1.15(2)	0.02(1)	4.19(2)	3.77(5)	14.16(13)	9.70(20)	1.35(5)	1.32(5)	12.94(17)
CaO	11.80(32)	7.74(8)	5.57(9)	8.78(45)	17.32(11)	15.89(9)	18.83(19)	16.78(44)	9.42(8)	7.23(9)	23.78(25)
Na_2O	12.51(26)	10.86(11)	7.53(11)	3.50(6)	2.41(5)	2.23(7)	2.06(7)	2.33(6)	16.81(39)	14.27(14)	1.26(5)
K_2O	1.15(8)	1.31(4)	1.30(3)	3.65(7)	1.31(3)	1.29(4)	0.66(3)	1.61(7)	1.27(4)	1.33(4)	0.41(3)
P_2O_5	6.33(58)	3.80(5)	2.49(7)	1.01(12)	3.40(1)	3.44(19)	4.85(19)	4.68(35)	4.87(20)	1.64(12)	8.57(26)
F	—	—	—	—	—	—	2.74(13)	—	2.46(12)	3.44(9)	—
Cl	0.33(1)	0.24(4)	0.17(1)	—	—	—	—	—	0.43(3)	0.35(2)	—
F·Cl=O	0.07	0.05	0.04	0.00	0.00	0.00	1.15	0.00	1.13	1.53	0.00
Total	91.07	91.74	88.58	94.37	97.22	94.01	98.88	93.73	98.42	97.91	97.86
ASI	0.118	0.298	0.596	0.618	0.441	0.446	0.418	0.386	0.125	0.286	0.328
n.o.a.	(3)	(3)	(3)	(1)	(2)	(3)	(3)	(4)	(3)	(5)	
Rb	329(3)	359(1)	364(22)	378(−)	251(1)	263(5)	670(6)	411(8)	360(7)	362(5)	—
Sr	64.7(2)	52.7(15)	51.6(32)	59.0(−)	73.1(1)	73.8(7)	197(1)	59.6(19)	73.1(23)	64.3(9)	—
Y	54.6(1)	43.3(22)	30.9(19)	35.4(−)	55.5(5)	52.8(12)	65.2(2)	62.4(32)	35.3(17)	34.1(2)	—
Zr	93.2(1)	200(2)	190(8)	154.3(−)	97.6(5)	144(3)	230(1)	108(1)	105(2)	103(1)	—
Nb	329(2)	384(4)	402(22)	410(−)	401(2)	288(14)	222(3)	359(5)	127(4)	268(3)	—
Cs	282(3)	293(2)	273(7)	264(−)	177(2)	508(12)	500(5)	334(5)	304(2)	294(4)	—
Ba	339(1)	384(7)	375(17)	426(−)	352(2)	268(13)	477(1)	332(7)	384(3)	374(4)	—
La	50.7(3)	33.9(6)	23.5(9)	40.2(−)	52.8(12)	52.6(17)	54.2(5)	54.7(31)	24.6(18)	22.5(2)	—
Ce	42.4(11)	28.9(9)	19.7(16)	30.0(−)	48.8(22)	53.9(73)	78.4(5)	47.2(29)	22.8(19)	19.2(3)	—
Pr	41.8(3)	28.2(6)	19.1(11)	36.6(−)	43.4(14)	45.2(12)	59.0(3)	37.8(23)	19.8(21)	17.7(3)	—
Sm	43.3(16)	28.0(4)	18.6(12)	32.7(−)	42.5(14)	43.6(19)	50.4(9)	44.5(29)	20.7(31)	16.8(2)	—
Gd	45.4(11)	30.7(3)	19.7(5)	25.2(−)	35.5(4)	33.1(5)	52.8(11)	49.1(35)	23.4(14)	19.8(8)	—
Lu	60.0(4)	56.3(4)	46.0(9)	49.8(−)	69.0(28)	65.8(12)	68.4(3)	59.5(17)	46.3(4)	47.7(5)	—
Hf	75.0(13)	83.5(18)	91.7(27)	86.0(−)	85.8(7)	82.5(31)	132(3)	98.2(9)	81.2(25)	80.0(11)	—
Ta	244(1)	279(1)	298(5)	292(−)	323(3)	310(3)	330(1)	228(5)	225(1)	262(4)	—
Pb	8.93(14)	74.4(1)	65.1(1)	72.7(−)	114(11)	160(3)	21.4(12)	83.9(25)	7.89(64)	7.00(99)	—
Th	86.4(8)	83.8(29)	74.2(17)	97.3(−)	66.6(9)	76.0(3)	176(1)	103(3)	85.1(9)	87.2(17)	—
U	137(18)	160(1)	165(2)	706(−)	67.1(15)	79(6)	234(7)	984(20)	147(2)	154(3)	—

n.o.a, number of analyses (x). cpfu, cations per formula unit. ASI, alumina saturation index (molar ratio: $Al_2O_3/(Na_2O + K_2O + CaO)$. All errors are 1σ, given as last significant digits in brackets. Note that traces of chlorine are also present due to contamination of the starting materials. Major elements were analysed with the electron microprobe, whereas trace elements were analysed using SIMS techniques (see text for analytical details).

Table 5
Trace element partition coefficients between apatite and different silicate melt

Sample	72	78	77	61B	71A	61A	48B	59B	43	54A	60B
Rb	0.0013(1)	0.0016(1)	0.0009(3)	0.0010(−)	0.0030(5)	0.0010(1)	0.0006(1)	0.0007(1)	0.0004(2)	0.0007(1)	—
Sr	2.43(12)	3.72(25)	5.10(38)	4.3(−)	1.45(1)	1.37(2)	1.10(1)	1.56(5)	3.79(14)	4.59(24)	—
Y	2.58(3)	3.82(16)	8.73(62)	7.1(−)	1.66(7)	2.91(8)	2.83(5)	3.92(20)	5.69(27)	8.43(27)	—
Zr	0.030(1)	0.041(1)	0.047(4)	0.042(−)	0.078(1)	0.056(2)	0.027(1)	0.069(2)	0.020(1)	0.030(2)	—
Nb	0.0012(1)	0.0018(1)	0.0023(2)	0.0011(−)	0.0035(17)	0.0024(1)	0.0012(1)	0.0022(1)	0.0011(1)	0.0013(7)	—
Cs	0.0002(1)	0.0002(1)	0.0001(1)	0.0001(−)	0.0002(1)	0.0001(1)	0.0001(1)	0.0002(1)	0.0002(1)	0.0003(1)	—
Ba	0.10(1)	0.14(1)	0.14(2)	0.12(−)	0.06(1)	0.06(1)	0.06(1)	0.05(1)	0.16(1)	0.18(1)	—
La	4.85(4)	8.33(27)	16.6(7)	11.4(−)	1.91(11)	2.94(10)	2.80(4)	4.32(26)	13.3(10)	19.7(11)	—
Ce	4.92(13)	8.49(28)	18.1(15)	12.9(−)	2.33(7)	3.23(44)	3.25(5)	5.17(32)	13.6(13)	20.2(14)	—
Pr	5.43(1)	9.68(33)	20.6(13)	13.5(−)	2.67(12)	3.86(14)	3.67(2)	5.94(37)	14.6(16)	23.6(21)	—
Sm	6.22(23)	11.4(21)	25.7(17)	16.1(−)	3.66(14)	5.68(25)	4.99(10)	8.25(57)	16.4(24)	28.3(29)	—
Gd	5.31(16)	9.12(8)	21.5(7)	13.9(−)	2.97(11)	5.13(9)	4.65(16)	7.44(54)	13.3(9)	22.1(23)	—
Lu	1.03(6)	1.39(8)	3.01(26)	3.92(−)	0.70(4)	1.22(8)	1.14(3)	1.62(7)	2.05(6)	2.94(8)	—
Hf	0.0065(13)	0.013(2)	0.012(1)	0.014(−)	0.020(1)	0.014(8)	0.010(1)	0.016(1)	0.0073(2)	0.0088(20)	—
Ta	0.0012(1)	0.0014(5)	0.0023(3)	0.0030(−)	0.0026(12)	0.0013(3)	0.0010(1)	0.0017(1)	0.0014(1)	0.0016(1)	—
Pb	0.64(11)	0.48(5)	0.94(19)	0.84(−)	0.29(8)	0.10(1)	0.39(3)	0.19(4)	0.62(5)	2.10(51)	—
Th	0.50(2)	0.65(3)	1.08(7)	1.28(−)	0.97(2)	0.70(3)	0.33(1)	0.95(5)	0.40(1)	0.47(1)	—
U	0.53(2)	0.25(2)	0.08(1)	1.40(−)	0.46(5)	0.17(1)	0.48(2)	0.70(4)	0.35(1)	0.34(1)	—
D_{La}/D_{Lu}	4.73	6.01	5.52	2.90	2.74	2.41	2.46	2.67	6.49	6.71	
D_{Zr}/D_{Hf}	4.62	3.22	4.00	2.90	3.89	3.98	2.74	4.22	2.67	3.45	
D_{Nb}/D_{Ta}	0.93	1.34	1.04	0.39	1.35	1.89	1.24	1.29	0.35	0.81	
D_{Th}/D_{U}	0.94	2.62	12.78	0.92	2.09	4.17	0.69	1.36	1.16	1.39	

Note some analytical and experimental problems with Pb (see text for further explanations); 1σ uncertainty quoted in terms of last significant digits.

Green (1981) and Klemme and Dalpe (2003). We find that Sr is compatible ($D > 1$), whereas all other trace elements are incompatible in apatite ($D < 1$). We find that $D_{Cs} < D_{Rb} < D_{Ba}$ and $D_{Zr} > D_{Hf} > D_{Nb} \approx D_{Ta}$. We also find that D_{Th} and D_{U} are close to unity, and in most cases $D_{Th} > D_{U}$. The U partition coefficients show some variation which is probably due to slight changes in oxygen fugacity. As we used graphite-lined capsules in our experiments we expect reducing conditions in all our runs hence mostly quadrivalent uranium (U^{4+}), but we cannot completely exclude some hexavalent U (U^{6+}) in our experiments. Our data show that D_{La} is always higher than D_{Lu}, regardless of melt composition. This is somewhat contrary to the findings of Watson and Green (1981) who report $D_{La} < D_{Lu}$ in very silicic compositions. Although our partition coefficients are in the same ballpark, we believe that these subtle differences may be due to different melt compositions. Note, however, that Watson and Green's (1981) experiments were conducted at much lower temperatures and at different pressure which may explain some of the observed differences.

Moreover, we also set out to investigate the effect of melt composition on REE partitioning between apatite and melt. This experimental approach is identical to previous studies where we set out to investigate the partitioning of trace elements between titanite, rutile and silicate melts (Prowatke and Klemme, 2005; Prowatke et al., 2004; Klemme et al., 2005). All our experiments were conducted at identical pressures (1.0 GPa) and temperatures (1250 °C). Moreover, the major element composition of our apatites is virtually constant, so that the only remaining variable in our experiments is melt composition.

Fig. 3 shows that REE partition coefficients increase with increasing degree of polymerisation of the melt. This observation is in good agreement with results by Watson and Green (1981) who found that REE partition coefficients in their systems increased with increasing SiO_2-content of the melt. However, our partition coefficients for univalent (Rb, Cs), divalent elements (Pb, Sr, and Ba), quadrivalent (Hf, Zr, U, and Th) and pentavalent elements (Nb, Ta) are not significantly affected by changing melt compositions (Fig. 3).

Previous studies have shown that trace element partition coefficients depend on pressure, temperature, crystal composition, and melt composition. As our experiments were preformed at constant pressure and temperature, we will discuss possible crystal chemical and melt compositional controls on apatite partitioning in the following paragraphs.

3.3. Crystal chemical controls on REE partitioning between apatite and melt

Rare earth elements (REE) can substitute for Ca in apatite. There are two different positions for the incorporation of REE available in the apatite structure (e.g., Hughes et al., 1989; Hughes et al., 1991; Hughes and Rakovan, 2002). The Ca(1) site is ninefold coordinated (CaO_9) with a multiplicity of 4. The Ca(2) site is sevenfold coordinated (CaO_6X, where X = F, Cl, or OH) with a multiplicity of 6. Fleet et al. (2000) suggested that the lattice energy on Ca(1) is dominated by a sixfold coordination of Ca only a small contribution from oxygen atoms in greater bond distance.

The structural formula of apatite may be written as (Fleet and Pan, 2000a):

$$Ca(1)_4^{VI+III}Ca(2)_6^{VII}(PO_4)_6X_2$$

The partition coefficients for the rare earth elements (REE, including Y^{3+}, which mimics the behaviour of the rare earth elements) show a convex-upward shape when plotted against ionic radius (Onuma et al., 1968). The peak of the REE pattern is in the near of Sm, which means that apatite prefers to incorporate the middle rare earth elements (MREE) relative to the light rare earth elements (LREE) and heavy rare earth elements (HREE) with slightly higher partition coefficients for the LREE (La, Ce, and Pr) compared to the HREE (Yb, Lu).

The distribution of REE between the two distinct Ca positions in apatite was discussed in several studies. For instance the study by Cockbain and Smith (1967) indicate no particular preference of all REE for either site. A preference of all REE only for Ca(1) was suggested by Urusov and Khudolozhkin (1974) whilst a preference only for Ca(2) was put forward by Borisov and Klevtsova (1963). A recent study by Hughes et al. (1991) who used bond valence theory showed a preference for the Ca(2) site for the LREE (La, Ce, and Pr). Furthermore, Hughes et al. (1991) suggested that Sm should prefer the Ca(1) site, whereas Nd was predicted to show no preference and should readily fit on both sites Ca(1) and Ca(2). Summarizing, the crystallographic results from Hughes et al. (1991) and Fleet and Pan (1997a) indicate that REE partition coefficients of apatite should display a concave downward pattern centered on Nd, with higher partition coefficients for the LREE compared to the HREE (Hughes et al., 1991). The crystallographic results agree well with our experimental results (Fig. 4). Nevertheless there are some differences when comparing our new data to some older experimental studies by Watson and Green (1981) and Fleet and Pan (1995) which may be largely due to differences in temperature and bulk composition.

In summary, we find that the influence of crystal structure on the apatite/melt partition coefficients can be neglected in our experiments, as our apatites have very low Na, Si, and REE trace element concentrations (Table 3) and the major element composition of the apatites in our experiments is identical. However, some apatites contained fluorine instead of OH^-. In the next paragraph, we will briefly evaluate a possible effect of halogens on trace element partitioning.

3.4. The influence of halogens on partitioning

Fleet and Pan (1997a) speculated that the volatile anion component (i.e., Cl^-, F^- or OH^-) plays an important role in the trace element uptake of apatite because of its proposed influence on the environment and the size of the Ca(2) site. We performed experiments with two different apatite compositions, i.e., F^-- and OH^--apatite to test this hypothesis.

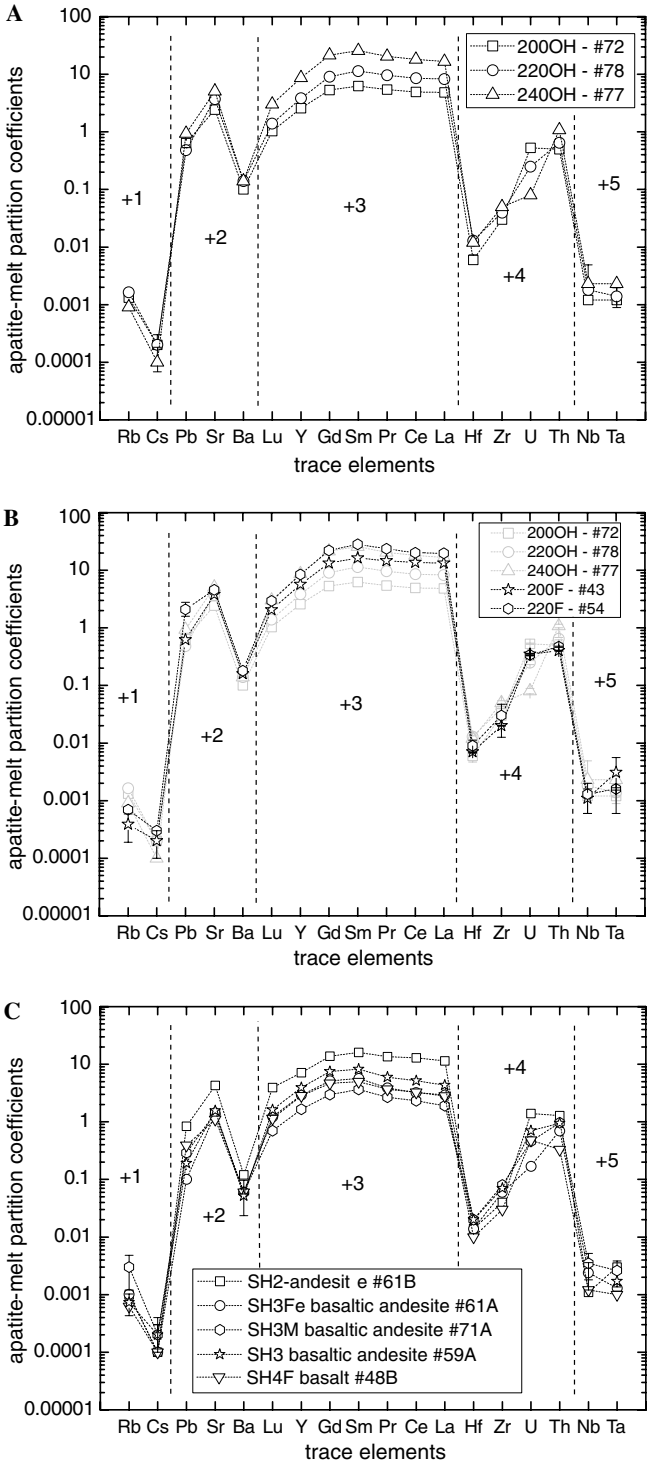

Fig. 3. Apatite/melt partition coefficients [D = c(crystal)/c(melt)] calculated from SIMS analyses of our experimental run products. (A) partition coefficients from H_2O-containing experiments. With increasing alumina saturation index (ASI—molar ratio: $Al_2O_3/(Na_2O + K_2O + CaO)$) of coexisting melts or increasing degree of polymerisation we observe substantial variations for the REE with only minor effects of melt composition on other elements. (B) Depicted are the partition coefficients of experiments that contain F instead of water. (C) Experimental results in systems approximating natural compositions. All three figures (A–C) show the same phenomenon that is increasing partition coefficients with increasing degree of polymerisation of the coexisting melt. See text for further discussion. Error bars only shown when they are larger than symbols.

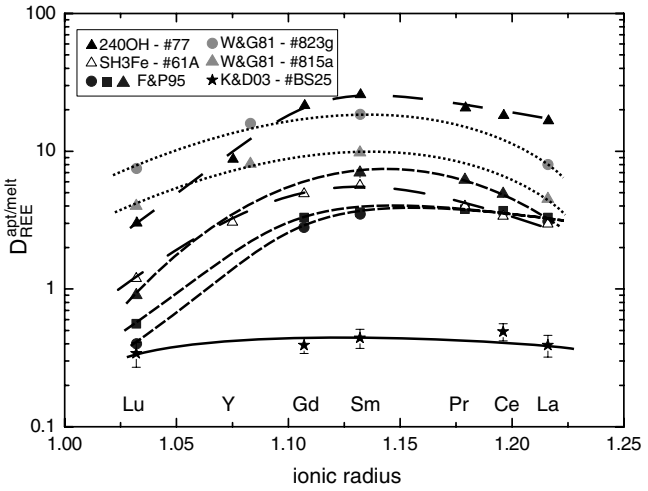

Fig. 4. Partition coefficients plotted against ionic radius (Onuma et al., 1968; Shannon, 1976). Depicted are our new experimental apatite/melt partition coefficients for selected REE and previous results from (Watson and Green, 1981 – W & G81; Fleet and Pan, 1995 F & P95; Klemme and Dalpe, 2003-K & D03). The general pattern of partition coefficients from our experiment SH3Fe (i.e., in a basaltic andesite composition) agrees well with the pattern observed by Watson and Green (1981) for silicate melts, although our D_{La}/D_{Lu} is somewhat higher. See text for further details.

However, the overall difference between the REE partition coefficients in fluorine- and water-bearing systems is rather small (Table 5). Therefore, it seems that the anion species on the Ca(2)-site has only a very small influence on the REE partitioning (Klemme and Dalpe, 2003).

3.5. The influence of substitution mechanisms on trace element partitioning between apatite and melt

Previous work suggested that the substitution mechanism, by which trace elements are incorporated into a crystal structure, may also control partition coefficients (e.g., Corgne and Wood, 2005; Prowatke and Klemme, 2006). Several possible exchange mechanisms have been reported for the incorporation of the REE and other elements into the apatite structure. For an excellent review on many possible substitution mechanism for apatite refer to Pan and Fleet (2002). In this section, we will concentrate on the incorporation of the REE into apatite. The following main substitution mechanisms are possible:

(1) $2REE^{3+} + [v] = 3Ca^{2+}$ (e.g., Chen et al., 2002; Fleet and Pan, 2003)
(2) $REE^{3+} + Si^{4+} = Ca^{2+} + P^{5+}$ (e.g., Watson and Green, 1981; Ronsbo, 1989)
(3) $REE^{3+} + Na^{+} = 2Ca^{2+}$ (e.g., Ronsbo, 1989) where [v] represents a cation vacancy. In all our experiments the sum of Na + Si exceeds the sum of REE in apatite. Similar observations were made by Roeder et al., 1987; Fleet and Pan, 1997a; and Klemme and Dalpe, 2003. However, although Na concentrations are very low (Table 3), we find slightly increasing Na in apatite with increasing Na in melts, and a slight decrease of Si in apatite with increasing Si in melts. This is consistent with the observations of Prowatke and Klemme (2005), who found virtually no dependence of the Al and Na concentration in titanite regardless of the presence or absence of trace elements in the bulk composition. Furthermore they observed that the sum of Na + Al is always larger than the sum of REE + Th in titanite (Prowatke and Klemme, 2005; Prowatke and Klemme, 2006). Therefore, the incorporation of Na into apatite must be controlled by another substitution mechanism, either
(4) $2Na^{+} = Ca^{2+} + [v]$ (e.g., Pan and Fleet, 2002) or
(5) $Na^{+} + [v] = Ca^{2+} + F^{-}$ or OH (e.g., Pan and Fleet, 2002). However, we see two trends in (Fig. 6). It appears that F-apatite incorporates clearly less Na_2O compared to apatites in melts with no fluorine (but water). Following Fleet and Pan (1997a,b) and Fleet et al. (2000), Na should favour the Ca(1) position and the Na incorporation should not be controlled by the volatile elements (which would only affect the Ca(2) position in apatite). However, a possible explanation for higher Na concentrations in apatite in fluorine-rich systems may be the complexation of Na with F. In contrast, we find Si contents in apatite slightly decreasing with increasing Si in melts (Tables 3, 4, Fig. 6B). The Si in apatite in trace and minor concentrations appears, therefore, most to be likely charge balanced by vacancies on the Ca or X position (the one occupied by volatile elements) along the lines of the following substitution mechanisms:
(6) $P^{5+} + OH^{-} = Si^{4+} + [v^{OH-}]$ (e.g., Schwarz, 1968)
(7) $P^{5+} + 3OH^{-} = Si^{4+} + O^{2-} + 2[v^{OH-}]$ (e.g., Trombe and Montel, 1978).

Fig. 6D shows that the H_2O-content of the melt and the absolute concentration of SiO_2 in apatite are correlated. With increasing water content of the melt the activity of SiO_2 in the melt decreases which could explain our observation depicted in Fig. 6D.

We conclude that the Na content in apatite is mainly controlled by the Na_2O content of the melt (Fig. 6A). This also holds for the Mg- and Fe-content in apatite (Fig. 6C). The Si content in apatite appears to depend on the H_2O content of the melt (Fig. 6D). The uptake of trace elements (e.g., REE) do not control the Na and Si content of apatites. This leads us to the conclusion that the substitution mechanism does not play a major role in controlling REE partition coefficients in our experiments.

3.6. The influence of melt composition on the partitioning of trace elements

Melt composition is known to exert a significant influence on the partitioning of trace elements between crystals and melts. Early partitioning experiments between immiscible silicate liquids were carried out by Watson (1976) and

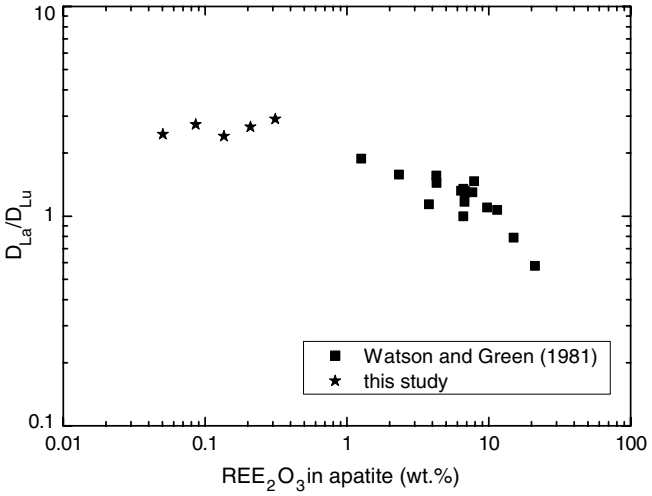

Fig. 5. The influence of the REE_2O_3 content in apatite on the D_{La}/D_{Lu} ratio. Depicted are the D_{La}/D_{Lu} ratios of all experiments from Watson and Green (1981) and our experiments in natural compositions. It seems that with increasing REE_2O_3 content in apatite the ratio of D_{La}/D_{Lu} decrease (black squares). See text for further details.

Ryerson and Hess (1978) aimed at identifying melt compositional controls on trace element partitioning. They found that *D*'s of highly charged cations (e.g., Zr, Th, and REE) decreased with increasing degree of polymerisation of the melt. Consequently, the partition coefficients of these elements should increase with increasing polymerisation of the melt. The large ion lithophile elements (LILE: Na, K, Cs, and Rb) which have a low ionic charge/ionic radius ratio, should show the opposite effect. According to Watson (1976) and Ryerson and Hess (1978), Sr or Ba should show no preference for either of these silicate melts, and partition coefficients for these elements were suggested to be independent of melt compositions. The applicability of Watson's (1976) and Ryerson and Hess's (1978) results to our systems is uncertain because our systems are rich in phosphorus which is known to strongly influence melt structures.

Furthermore, Prowatke and Klemme (2005) suggest from their titanite/melt partitioning experiments that the structural environment of trace elements in melts could be of additional importance in this context. They suggested

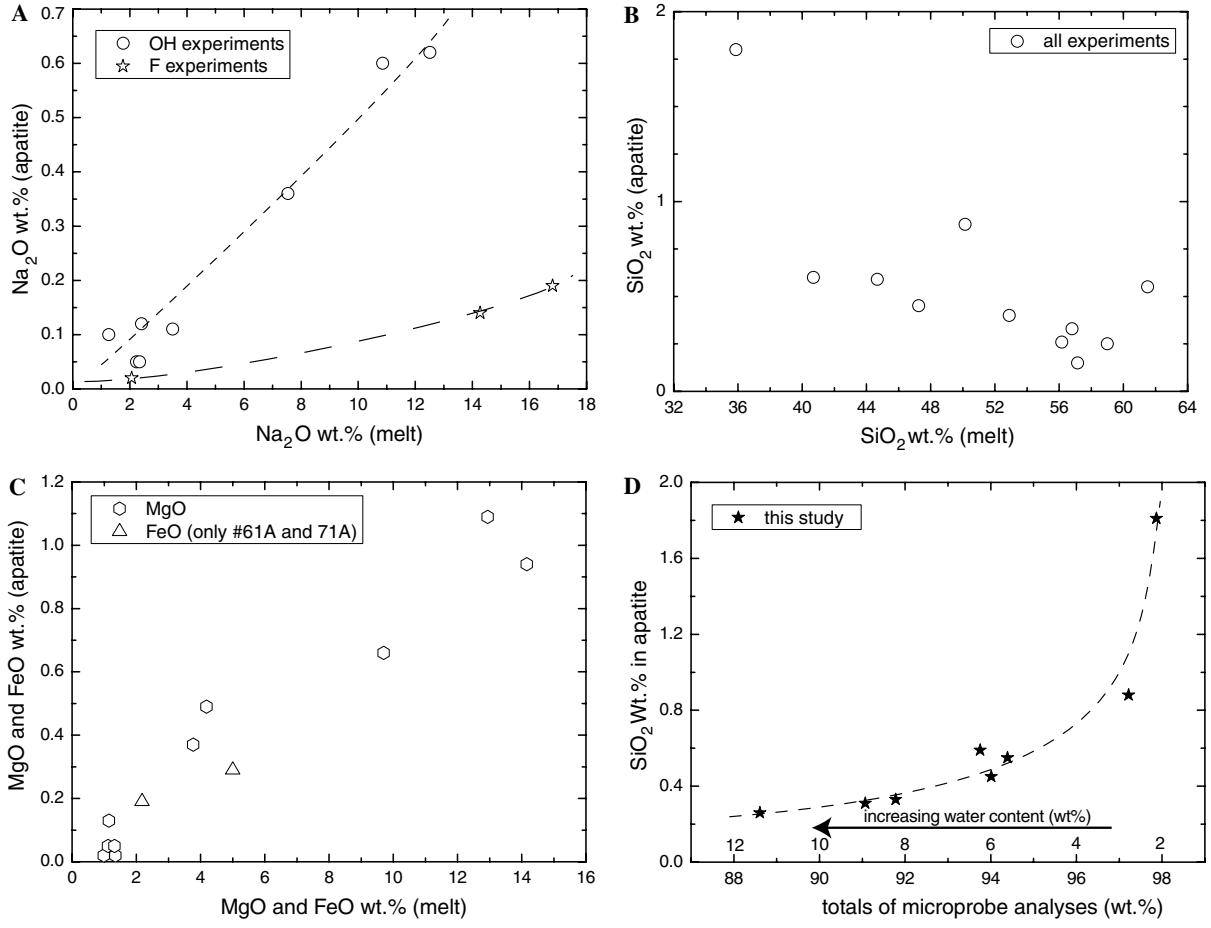

Fig. 6. Major element systematics of apatites and melts (A) We find increasing Na in apatite with increasing Na_2O content of the melt. Stars depict results from the experiments with F, and the open circles results from experiments with H_2O. The F-apatites exhibit much lower Na contents when compared to the OH-apatites. This could be due to complexation of F with Na in the melt—see text for discussion. (B) The SiO_2-content of melts plotted against the SiO_2-content in apatite. It seems that the silica content of apatite decreases slightly with increasing SiO_2-content in melt but the correlation is not great. (C) Variation of Mg (pentagons) and Fe (triangles) in apatite with increasing MgO and FeO content of the coexisting melt. See text for further discussion. (D) The influence of the dissolved water in melt on silica in apatite. Note that the water content was estimated from electron microprobe analyses. We observe increasing silica with decreasing H_2O content in melts. See text for further discussion.

that the coordination of some trace elements (REE, Th, Nb, and Ta) in melts varies with increasing degree of polymerisation, whereas the structural environment of trace elements like Zr or Sr are not affected by changing melt compositions. Recent observations using extended X-ray absorption fine structure (EXAFS: Ponader and Brown, 1989; Farges, 1991a,; Wilke et al., 2005) support Prowatke and Klemme's (2005) results.

3.7. Trace element partitioning between immiscible silicate and phosphate melts

Along the lines of the aforementioned studies on immiscible silicate liquid partitioning, we conducted an additional exploratory experiment to further investigate melt compositional effects on partition coefficients in phosphorus-rich system which may be more applicable to our apatite/melt partitioning experiments. We equilibrated immiscible phosphate and silicate melts experimentally (Fig. 8A and B) and found that the large ion lithophile elements prefer to partition into the silicate melt, whereas Sr, Ba, the REE, and U preferentially partition into the phosphate melt and the quadrivalent and pentavalent elements show no preference for either melt. Our liquid–liquid experiment (Fig. 7, Table 6) indicates a slight fractionation between the REE, with the LREE slightly more compatible in the phosphate melt than the HREE which is in good agreement with our results from apatite/melt partitioning (Fig. 5). Ellison and Hess (1989) found no fractionation between the REE in silicate melt–silicate melt experiments,

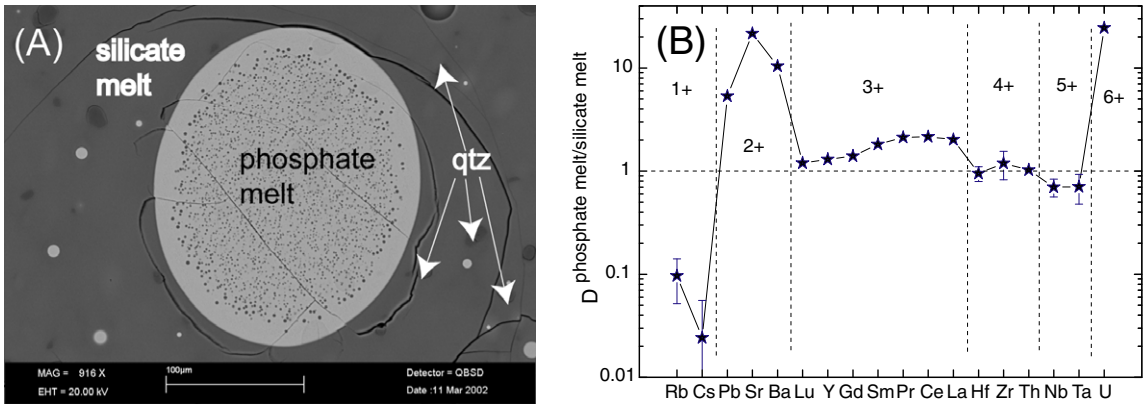

Fig. 7. (A) Backscattered electron image showing three different phases coexisting: quenched phosphate melt, quenched silicate melt, and SiO_2 crystals. The immiscible blebs of the phosphate melts vary from mm to µm in size. The centre of the phosphate glass blebs contains numerous very small inclusions (1–3 µm in size) of silicate glass. The quartz crystals are only present in the silicate glass and are usually smaller than 10 µm. Note that the cracks are caused by the quench. (B) Phosphate melt/silicate melt partition coefficients calculated from LA-ICPMS analyses of these run products. The divalent, trivalent and hexavalent cations are strongly compatible in phosphate melt, whereas the monovalent cations show a very incompatible behaviour. The quadri- and pentavalent cations show no preference for either melt. Note that the experiment was carried out at atmospheric pressure and at temperatures of 1510 °C. See text for details.

Table 6
Major element composition (wt%), trace element composition (ppm) of the coexisting melts and calculated trace element partition coefficients between phosphate melt and silicate melt

	Phosphate melt	Silicate melt	Trace	Phosphate melt	Silicate melt	Partition coefficient
SiO_2	1.9	77.0	Rb	24.5(9)	254(5)	0.096(44)
Al_2O_3	6.3	13.0	Cs	5.4(2)	224(4)	0.024(47)
Na_2O	1.3	2.7	Pb	147(40)	27.5(3)	5.34(30)
K_2O	0.3	4.2	Sr	234(3)	10.8(7)	21.6(1)
CaO	42.0	1.2	Ba	1491(44)	142(20)	10.4(1)
P_2O_5	49.0	0.6	Lu	29.7(16)	33.2(47)	1.20(14)
			Y	34.3(19)	26.3(31)	1.30(13)
Total	100.8	98.7	Gd	45.1(15)	32.2(46)	1.40(15)
			Sm	54.8(37)	30.1(35)	1.81(14)
			Pr	81.6(45)	38.5(51)	2.12(14)
			Ce	98.4(58)	45.6(57)	2.15(14)
			La	88.7(47)	43.8(61)	2.02(15)
			Hf	45.6(10)	48.1(70)	0.95(15)
			Zr	59.5(4)	50(18)	1.19(36)
			Th	60.4(21)	59.0(75)	1.02(13)
			Nb	174(7)	249(32)	0.70(14)
			Ta	124(3)	176(39)	0.70(22)
			U	1055(30)	43.1(34)	24.4(8)

1σ uncertainty quoted in terms of last significant digits – 1σ uncertainty by normal error propagation.

but this may be due to different melt compositions. On the other hand, REE fractionation between immiscible liquids was recently observed by Klemme (2004) and Veksler et al. (1998, 2004, 2005). Furthermore, van Westrenen et al. (2000) show in a computer simulation study of garnet-melt partitioning that the fractionation between the REE may be influenced by the structure of the coexisting melt. This was supported by Prowatke and Klemme (2005), who show in a systematic partitioning study that changes of the structural environment of REE in melts could result in fractionation between REE.

The liquid–liquid partitioning experiment also indicates that the quadrivalent and pentavalent elements (i.e., with valence states of 4 and 5) show no preference for either of the coexisting melts. This observation contrasts findings by Ryerson and Hess (1978) in systems with very little phosphorus but may well explain the fact that our Zr and Hf apatite–liquid partition coefficients are not affected by changing melt compositions. The divalent elements in our liquid–liquid partitioning experiment are highly compatible in the phosphate melt. The reason for this could be the structure of the phosphate melt, which consists primarily of Ca^{2+} and P^{5+}. Sr^{2+} and Ba^{2+} exhibit a very similar chemical behaviour as Ca^{2+} and should, therefore, stabilize the phosphate network. Partition coefficients of Sr and Ba between apatite and melt are strongly correlated with the CaO content of the melt (Fig. 8B and C) and we observe a strong decrease of D_{Sr} and D_{Ba} with increasing CaO content in the melt. The substitution mechanism cannot be responsible for this behaviour, as Sr and Ba are incorporated into apatite along the lines of a homovalent substitution for Ca.

In conclusion, our new experimental data clearly shows that melt composition exerts a significant influence on the partition coefficients for the REE. We find that REE partition coefficients increase with increasing degree of polymerisation of the melt (Fig. 8A) whereas partition coefficients for all other elements studied remain largely unaffected by changing melt composition.

4. Applications to natural compositions

Most of our experiments were conducted in synthetic compositions to investigate the effect of bulk composition on partition coefficients. However, we conducted several experiments in systems rather close to natural rock compositions (Table 1). We would, therefore, recommend the use of partition coefficients from these compositions for geochemical calculations.

In fractionating systems, however, when apatite crystallizes from melts with changing compositions, one could

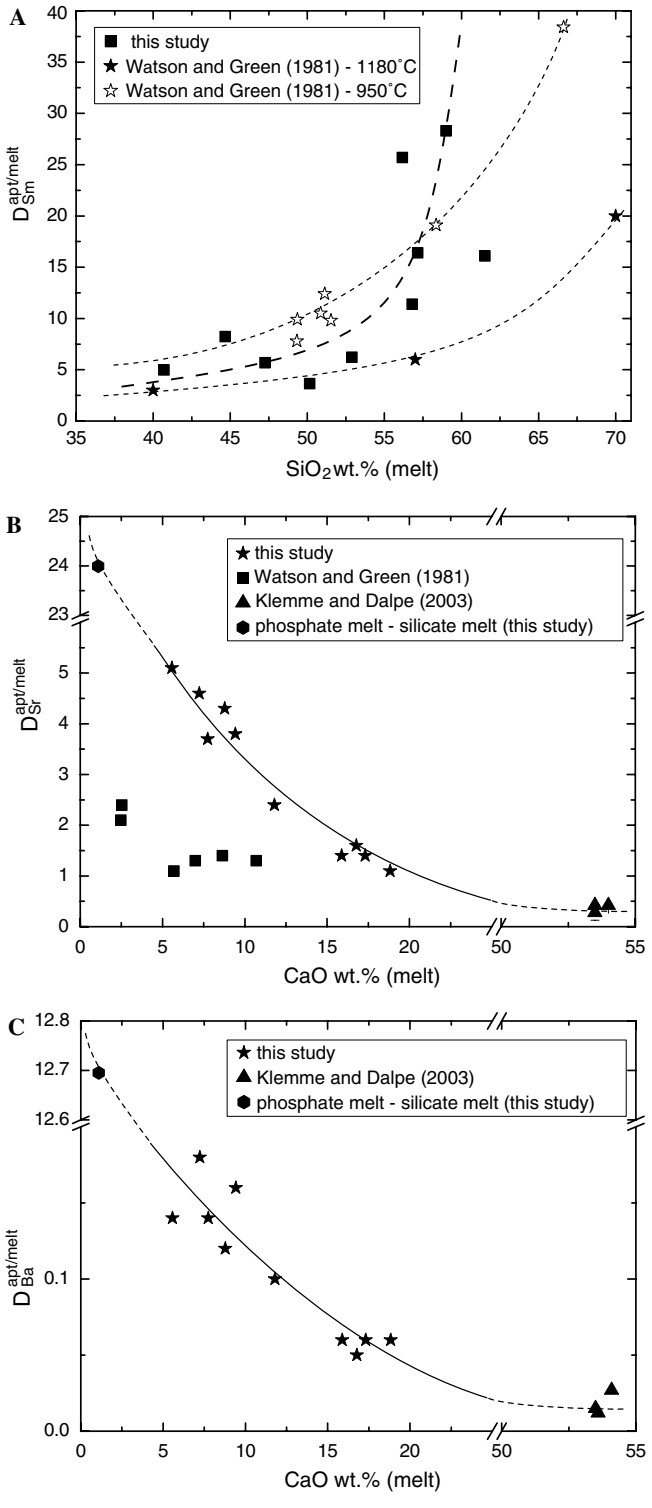

Fig. 8. (A) Variation of D_{Sm} with SiO_2 content of the melt. The stars represent experimental results from Watson and Green (1981) at different temperatures. With decreasing temperature the Sm partition coefficients between apatite and melt increase. The black squares show trends from our experiments, which roughly agree with results by Watson and Green (1981). See text for further discussion. (B) Variation of D_{Sr} and (C) D_{Ba} with increasing CaO content (wt.%) of melt. D_{Ba} and D_{Sr} decrease strongly with increasing CaO content. The triangles depict D_{Ba} and D_{Sr} from partition experiments between apatite and carbonate melt (Klemme and Dalpe, 2003), whereas the hexagon shows the results from our new phosphate liquid–silicate liquid experiment for Sr and Ba. The results indicate that the partitioning of Ba and Sr depends on the Ca content of the melt. Note that some experiments by Watson and Green (1981) seem not to fit in the observed trends which may be due to differences in temperature and/or bulk composition.

certainly use trends observed in the experiments with systematically changing melt compositions. For example, consider the case where apatite crystallizes slowly during the cooling of a magmatic system. Based on the partitioning systematics (increasing D_{REE} with increasing degree of polymerization of the melt) one would expect increasing REE concentrations from core to rim of zoned apatite crystals. The interpretation of zoned accessory phases in magmatic systems is, of course, much more complex than this but our partition coefficients may help to shed further light on the complexity of evolving magmatic systems.

As an example, we would like to point out that our experiments may also be used to explain some geochemical signatures of naturally occurring apatite phenocrysts. Our partition coefficients indicate that D_{Sr} is higher than D_{Sm} (or other REE) in depolymerised melts with low Ca concentration (Tables 4 and 5). In contrast, D_{Sr} is much smaller in most other melt compositions. If one assumes that Sr behaves in an identical manner to Eu (Watson and Green, 1981), this difference in partitioning behaviour could explain positive Eu anomalies in apatites in certain Ca-poor volcanics, whereas commonly observed negative Eu anomalies could both be explained by the apatite/melt partitioning of trace elements or, of course, by crystallization of feldspar (e.g., Bea et al., 1994).

5. Conclusions

We present a large number of hitherto unknown trace element partition coefficients for apatite in a range of different silicate melts. We find a strong influence of melt composition on partition coefficients: The rare earth element partition coefficients increase for about an order of magnitude with increasing degree of polymerisation of the melt, whereas apatite/melt partition coefficients for other elements are not affected significantly by changing melt composition.

Acknowledgments

We are indebted to Hans-Peter Meyer for his help with the electron microprobe at Heidelberg University. Furthermore, we would like to thank T. Zack, R. Altherr, T. Ludwig, Erfolgsgruppe 2000 and many others at Heidelberg University for discussions and support at various stages of the project. Our thanks also go to I. Fin and O. Wienand for their sterling efforts with sample preparation. Furthermore, we would like to thank Y. Lahaye and G. Brey for access to the Laser Ablation ICPMS at Frankfurt University. We are indebted to D. Lattard for access to the experimental laboratories at Heidelberg University. We would also like to thank Drs. E.B. Watson, M. Tiepolo and an anonymous reviewer for helpful comments on the manuscript. This research was in part supported by the Deutsche Forschungsgemeinschaft (KL1368/2-1).

Associate editor: Claudia Romano

References

Amelin, Y., Zaitsev, A.N., 2002. Precise geochronology of phoscorites and carbonatites: the critical role of U-series disequilibrium in age interpretations. *Geochim. Cosmochim. Acta* **66** (13), 2399–2419.

Bea, F., Pereira, M.D., Stroh, A., 1994. Mineral leucosome trace-element partitioning in a peraluminous migmatite (a laser ablation-ICP-MS study). *Chem. Geol.* **117** (1-4), 291–312.

Beswick, A.E., Carmichael, I.S.E., 1978. Constraints on mantle source compositions imposed by phosphorus and the rare earth elements. *Contrib. Mineral. Petrol.* **67**, 317–330.

Bohlen, S.R., Essene, E.J., Boettcher, A.L., 1980. Reinvestigation and application of olivine–quartz–orthopyroxene barometry. *Earth Planet. Sci. Lett.* **47**, 1–10.

Borisov, S.V., Klevtsova, R.F., 1963. The crystal structure of REE–Sr apatite. *Zh. Strukt. Khim.* **4**, 629–631.

Brigatti, M.F., Malferrari, D., Medici, L., Ottolini, L., Poppi, L., 2004. Crystal chemistry of apatites from the Tapira carbonatite complex, Brazil. *Eur. J. Miner.* **16** (4), 677–685.

Chazot, G., Menzies, M.A., Harte, B., 1996. Determination of partition coefficients between apatite, clinopyroxene, amphibole, and melt in natural spinel lherzolites from Yemen: implications for wet melting of lithospheric mantle. *Geochim. Cosmochim. Acta* **60** (3), 423–437.

Chen, N., Pan, Y., Weil, J.A., Nilges, M.J., 2002. Electron paramagnetic resonance spectroscopic study of synthetic fluorapatite: Part II. Gd at the Ca1 site and association with vacancy at Ca2 site. *Am. Miner.* **87**, 47–55.

Cockbain, A.G., Smith, G.V., 1967. Alkaline-Earth—rare earth silicate and germanate apatites. *Miner. Mag.* **36**, 411–421.

Corgne, A., Wood, B.J., 2005. Trace element partitioning and substitution mechanisms in calcium perovskites. *Contrib. Mineral. Petrol.* **149**, 85–97.

Dawson, J.B., 2002. Metasomatism and partial melting in upper-mantle peridotite xenoliths from the Lashaine volcano, northern Tanzania. *J. Petrol.* **43** (9), 1749–1777.

Dawson, J.B., Hinton, R.W., 2003. Trace-element content and partitioning in calcite, dolomite and apatite in carbonatite, Phalaborwa, South Africa. *Miner. Mag.* **67** (5), 921–930.

Dawson, J.B., Steele, I.M., Smith, J.V., Rivers, M.L., 1996. Minor and trace element chemistry of carbonates, apatites and magnetites in some African carbonatites. *Miner. Mag.* **60**, 415–425.

D'Orazio, M., Armienti, P., Cerretini, S., 1998. Phenocryst/matrix trace-element partition coefficients for hawaiite–trachyte lavas from the Ellittico volcanic sequence (Mt. Etna, Sicily, Italy). *Mineral. Petrol.* **64** (1-4), 65–88.

Ellison, A.J.G., Hess, P.C., 1989. Solution properties of rare earth elements in silicate melts: Inreferences from immiscible liquids. *Geochim. Cosmochim. Acta* **53**, 1965–1974.

Farges, F., 1991a. Structural environment around Th^{4+} in silicate glasses—implications for the geochemistry of incompatible Me^{4+} elements. *Geochim. Cosmochim. Acta* **55** (11), 3303–3319.

Farges, F., Ponader, C.W., Brown, G.E., 1991. Structural environments of incompatible elements in silicate glass melt systems. 1. Zirconium at trace levels. *Geochim. Cosmochim. Acta* **55** (6), 1563–1574.

Fleet, M.E., Liu, X.Y., Pan, Y., 2000. Site preference of rare-earth elements in hydroxyapatite [$Ca_{10}(PO_4)_6(OH)2$]. *J. Solid State Chem.* **149**, 391–398.

Fleet, M.E., Pan, Y., 1995. Site preference of rare earth elements in fluoeapatite. *Am. Miner.* **80**, 329–335.

Fleet, M.E., Pan, Y.M., 1997a. Rare earth elements in apatite: uptake from H_2O-bearing phosphate-fluoride melts and the role of volatile components. *Geochim. Cosmochim. Acta* **61** (22), 4745–4760.

Fleet, M.E., Pan, Y.M., 1997b. Site preference of rare earth elements in fluorapatite: binary (LREE + HREE)-substituted crystals. *Am. Miner.* **82** (9-10), 870–877.

Fujimaki, H., 1986. Partition-coefficients of Hf, Zr, and REE between zircon, apatite, and liquid. *Contrib. Mineral. Petrol.* **94** (1), 42–45.

Haggerty, S.E., Fung, A.T., Burt, D.M., 1994. Apatite, phosphorus and titanium in eclogitic garnet from the upper mantle. *Geophys. Res. Lett.* **21** (16), 1699–1702.

Harrison, T.M., Watson, E.B., 1984. The behavior of apatite during crustal anatexis—-equilibrium and kinetic considerations. *Geochim. Cosmochim. Acta* **48** (7), 1467–1477.

Hughes, J.M., Cameron, M., Crowley, K.D., 1989. Structural variations in natural F, OH, and Cl apatites. *Am. Miner.* **74**, 870–876.

Hughes, J.M., Cameron, M., Mariano, A.N., 1991. Rare-earth element ordering and structural variations in natural rare-earth-bearing apatites. *Am. Miner.* **76**, 1165–1173.

Hughes, J.M., Rakovan, J., 2002. The crystal structure of apatite, $Ca_5(PO_4)_3(F, OH,Cl)$. In: Kohn, M.J., Rakovan, J., Hughes, J.M. (Eds.), *Phosphates—Geochemical, Geobilogical and Materials Importance*, Vol. 48. Mineralogical Society of America, pp. 1–11.

Klemme, S., 2004. Evidence for fluoride melts in Earth's mantle formed by liquid immiscibility. *Geology* **32**, 441–444.

Klemme, S., Blundy, J.D., Wood, B.J., 2002. Experimental constraints on major and trace element partitioning during partial melting of eclogite. *Geochim. Cosmochim. Acta* **66**, 3109–3123.

Klemme, S., Dalpe, C., 2003. Trace-element partitioning between apatite and carbonatite melt. *Am. Miner.* **88**, 639–646.

Klemme, S., O'Neill, H.S.C., 1997. The reaction $MgCr_2O_4+SiO_2=Cr_2O_3+MgSiO_3$ and the free energy of formation of magnesiochromite ($MgCr_2O_4$). *Contrib. Mineral. Petrol.* **130**, 59–65.

Klemme, S., Prowatke, S., Hametner, K., Günther, D., 2005. The partitioning of trace elements between rutile and silicate melts: implications for subduction zones. *Geochim. Cosmochim. Acta* **69**, 2361–2371.

Kogarko, L.N., Krigman, L.D., Krot, T.V., 1988. The solubility and geochemistry of phosphorus in magmas. *Geochem. Int.* **25**, 1–12.

Krigman, L.D., Krot, T.V., 1992. Stable phosphate–silicate immiscibility in magmas. *Geochem. Int.* **29**, 28–41.

Mahood, G.A., Stimac, J.A., 1990. Trace-element partitioning in pantellerites and trachytes. *Geochim. Cosmochim. Acta* **54**, 2257–2276.

Nag, S., Sengupta, S.K., Gaur, R.K., Absar, A., 1999. Alkaline rocks of Samchampi-Samteran, District Karbi-Anglong, Assam, India. *Proc. Ind. Acad. Sci. Earth Planet. Sci.* **108** (1), 33–48.

Nagasawa, H., 1970. Rare Earth concentrations in zircon and apatite and their host dacite and granites. *Earth Planet. Sci. Lett.* **9**, 359–364.

Nagasawa, H., Schnetzler, C.C., 1971. Partitioning of rare Earth, alkali, and alkaline Earth elements between phenocrysts and acidic igneous magmas. *Geochim. Cosmochim. Acta* **35**, 953–968.

Nishizawa, M., Terada, K., Ueno, Y., Sano, Y., 2004. Ion microprobe U–Pb dating and REE analysis of apatite from kerogen-rich silica dike from North Pole area, Pilbara Craton, Western Australia. *Geochem. J.* **38**, 243–254.

Onuma, N., Higuchi, H., Wakita, H., Nagasawa, H., 1968. Trace element partitioning between two pyroxenes and the host lava. *Earth Planet. Sci. Lett.* **5**, 47–51.

O'Reilly, S.Y., Griffin, W.L., 2002. Apatite in the mantle: implications for metasomatic processes and high heat production in Phanerozoic mantle. *Lithos* **53**, 217–232.

Pan, Y., Fleet, M.E., 2002. Compositions of the apatite-group minerals: substitution mechanisms and controlling factors. In: Kohn, M.J., Rakovan, J., Hughes, J.M. (Eds.), *Phosphates—Geochemical, Geobilogical and Materials Importance*, Vol. 48. Mineralogical Society of America, pp. 13–49.

Parat, F., Holtz, F., 2004. Sulfur partitioning between apatite and melt and effect of sulphur on apatite solubility at oxidizing conditions. *Contrib. Mineral. Petrol.* **147** (2), 201–212.

Paster, T.P., Schauwecker, D.S., Haskin, L.A., 1974. The behavior of some trace elements during solidification of the Skaergaard layered series. *Geochim. Cosmochim. Acta* **38** (10), 1549–1577.

Pearce, N.J.G., Perkins, W.T., Westgate, J.A., Gorton, M.P., Jackson, S.E., Neal, C.R., Chenery, S.P., 1997. A compilation of new and published major and trace element data for NIST SRM 610 and NIST SRM 612 glass reference material. *Geostand. Newsl.* **21**, 115–144.

Piccoli, P., Candela, P., 1994. Apatite in Felsic rocks—a model for the estimation of initial halogen concentrations in the Bishop Tuff (Long Valley) and Tuolumne Intrusive Suite (Sierra-Nevada Batholith) Magmas. *Am. J. Sci.* **294** (1), 92–135.

Pichavant, M., Montel, J.M., Richard, L.R., 1992. Apatite solubility in peraluminous liquids—experimental-data and an extension of the Harrison–Watson model. *Geochim. Cosmochim. Acta* **56** (10), 3855–3861.

Ponader, C.W., Brown, G.E., 1989. Rare-Earth elements in silicate glass melt systems. 1. Effects of composition on the coordination environments of La, Gd, and Yb. *Geochim. Cosmochim. Acta* **53** (11), 2893–2903.

Pouchou, J.L., Pichoir, F., 1985. 'PAP' procedure for improved quantitative microanalysis. *Microbeam Anal.* **54**, 104–106.

Prowatke, S., Klemme, S., 2006. Rare earth element partitioning between titanite and silicate melts: Henry's law revisited. *Geochim. Cosmochim. Acta*, in press.

Prowatke, S., Klemme, S., 2005. Effect of melt composition on the partitioning of trace elements between titanite and silicate melt. *Geochim. Cosmochim. Acta* **69** (3), 695–709.

Prowatke, S., Klemme, S., Ludwig, T., 2004. Experimental constraints on the partitioning of trace elements between apatite and silicate melts. *Lithos* **73** (1-2), S91.

Raimbault, L., Baumer, A., Dubru, M., Benkerrou, C., Croze, V., Zahm, A., 1993. REE fractionation between scheelite and apatite in hydrothermal conditions. *Am. Miner.* **78** (11-12), 1275–1285.

Roeder, P.L., MacArthur, D., Ma, X.P., Palmer, G.R., 1987. Cathodoluminescence and microprobe study of rare earth elements in apatites. *Am. Miner.* **72**, 801–811.

Ronsbo, J.G., 1989. Coupled substitution involving REEs and Na and Si in apatites in alkaline rocks from the Illimaussaq intrusions, South Greenland, and petrological implications. *Am. Miner.* **74**, 896–901.

Ryabchikov, I.D., Edgar, A.D., Wyllie, P.J., 1991. Partial melting in a carbonatephosphate–peridotite system at 30 kbar. *Geokhimiya* **2**, 163–168.

Ryerson, F.J., Hess, P.C., 1978. Implications of liquid–liquid distribution coefficients to mineral–liquid partitioning. *Geochim. Cosmochim. Acta* **42** (A6), 921–932.

Schwarz, H., 1968. Strontium apatite des types $Sr_{10}(PO_4)_4(XIVO_4)_2$ (XIV=Si, Ge). *Z. Anorg. Allgem. Chem.* **357**, 43–53.

Seifert, W., Kampf, H., Wasternack, J., 2000. Compositional variation in apatite, phlogopite and other accessory minerals of the ultramafic Delitzsch complex, Germany: implication for cooling history of carbonatites. *Lithos* **53** (2), 81–100.

Shannon, R.D., 1976. Revised effective ionic radii and systematic studies of interatomic distances in halides and chalcogenides. *Acta Crystallogr.* **32**, 751–767.

Sorensen, S.S., Grossman, J.N., 1993. Accessory minerals and subduction metasomatism: a geochemical comparison of two melanges (Washington and California, USA). *Chem. Geol.* **110**, 269–297.

Trombe, J.-C., Montel, G., 1978. Some features of the incorporation of oxygen in different oxidation states in the apatite lattice-II. On the synthesis and properties of calcium and strontium peroxiapatites. *J. Inorg. Nucl. Chem.* **40**, 23–26.

Urusov, V.S., Khudolozhkin, V.O., 1974. An energy analyses of cation ordering in apatite. *Geochem. Int.* **11**, 1048–1053.

van Westrenen, W., Allan, N.L., Blundy, J.D., Purton, J.A., Wood, B.J., 2000. Atomistic simulation of trace element incorporation into garnets-comparison with experimental garnet-melt partitioning data. *Geochim. Cosmochim. Acta* **64** (9), 1629–1639.

Veksler, I.V., 2004. Liquid immiscibility and its role at the magmatic-hydrothermal transition: a summary of experimental studies. *Chem. Geol.* **210**, 7–31.

Veksler, I.V., Dorfman, A.M., Kamenetsky, M., Dulski, P., Dingwell, D.B., 2005. Partitioning of lanthanides and Y between immiscible silicate and fluoride melts, fluorite and cryolite and the origin of the lanthanide tetrad effect in igneous rocks. *Geochim. Cosmochim. Acta* **69**, 2847–2860.

Veksler, I.V., Petibon, C., Jenner, G.A., Dorfman, A.M., Dingwell, D.B., 1998. Trace element partitioning in immiscible silicate–carbonate liquid systems: an initial experimental study using a centrifuge autoclave. *J. Petrol.* **39**, 2095–2104.

Watson, E.B., 1976. Two-liquid partition-coefficients—experimental data and geochemical implications. *Contrib. Mineral. Petrol.* **56** (1), 119–134.

Watson, E.B., 1979. Apatite saturation in basic to intermediate magmas. *Geophys. Res. Lett.* **6** (12), 937–940.

Watson, E.B., 1980. Apatite and phosphorus in mantle source regions: an experimental study of apatite/melt equilibria at pressures to 25 kbar. *Earth Planet. Sci. Lett.* **51**, 322–335.

Watson, E.B., Green, T.H., 1981. Apatite/liquid partition coefficients for the rare-earth elements and strontium. *Earth Planet. Sci. Lett.* **56**, 405–421.

Wilke, M., Prowatke, S., Klemme, S. (2005). Determination of the local structural environment of trace elements in silicate glasses. HASYLAB report.

Wolf, M.B., London, D., 1994. Apatite dissolution into peraluminous haplogranitic melts: an experimental study of solubilities and mechanisms. *Geochim. Cosmochim. Acta* **58**, 4127–4145.

Yaxley, G.M., Green, D.H., Kamenetsky, V., 1998. Carbonatite metasomatism in the southeastern Australian lithosphere. *J. Petrol.* **39** (11-12), 1917–1930.